Temperature and Parasitic Photocurrent Effects in Dynamic Vision Sensors

Yuji Nozaki and Tobi Delbruck, *Fellow, IEEE*

***Abstract*— The effect of temperature and parasitic photocurrent on event-based dynamic vision sensors (DVS) is important because of their application in uncontrolled robotic, automotive, and surveillance applications. This paper considers the temperature dependence of DVS threshold temporal contrast (TC), dark current, and background activity caused by junction leakage. New theory shows that if bias currents have a constant ratio, then ideally the DVS threshold TC is temperature independent, but the presence of temperature dependent junction leakage currents causes nonideal behavior at elevated temperature. Both measured photodiode dark current and leakage induced event activity follow Arhenius activation. This paper also defines a new metric for parasitic photocurrent quantum efficiency and measures the sensitivity of DVS pixels to parasitic photocurrent.**

***Index Terms*— CMOS image sensors, dark current, junction leakage, photocurrent, vision sensor.**

I. Introduction

DYNAMIC vision sensors (DVS) and related sensors output asynchronous temporal contrast (TC) address events that signal local pixel-level brightness change [1]–[9]. Because DVS have sparse, quick, and high dynamic range output, they can overcome the limited dynamic range and latency-power tradeoff of frame-based cameras, and are being developed for applications in surveillance, robotics, and scientific imaging [11], [12].

So far, there has been no study of temperature dependence of DVS sensor variants. Because of the applications of DVS in uncontrolled environments, the main purpose of this paper is to model and measure the effect of temperature on DVS. In addition, unintended photocurrent in MOS transistor source/drain junctions (parasitic photocurrent) causes event activity in the presence of strong dc lighting. This effect is closely related to junction leakage current temperature dependent effects.

Manuscript received April 4, 2017; revised May 12, 2017; accepted June 9, 2017. Date of publication June 29, 2017; date of current version July 21, 2017. This work was supported in part by the European projects VISUALISE under Grant FP7-ICT-600954, in part by SEEBETTER under Grant FP7-ICT-270324, and in part by the Tokyo Tech Exchange Program of the Tokyo Institute of Technology. The review of this paper was arranged by Editor A. Lahav. *(Corresponding author: Tobi Delbruck.)*

Y. Nozaki was with the Institute of Neuroinformatics, CH-8057 Zürich, Switzerland, and inilabs GmbH, CH-8057 Zürich, Switzerland. He is now with the Tokyo Institute of Technology, Kanagawa 226-8503, Japan (e-mail: nozaxi0327@gmail.com).

T. Delbruck is with the Institute of Neuroinformatics, University of Zurich, CH-8057 ETH Zürich, Switzerland, and also with inilabs GmbH, CH-8057 Zürich, Switzerland (e-mail: tobi@ini.uzh.ch).

Color versions of one or more of the figures in this paper are available online at http://ieeexplore.ieee.org.

Digital Object Identifier 10.1109/TED.2017.2717848

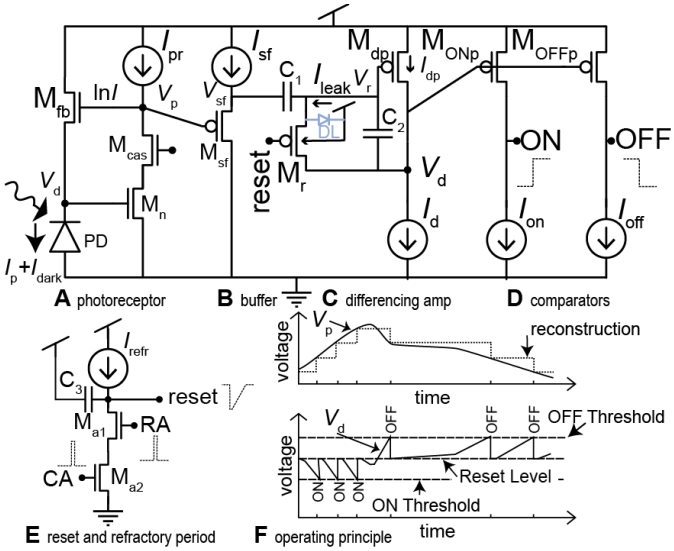

Fig. 1. DVS pixel and operation. (A)–(E) Analog part of original DVS pixel circuit. The digital circuits that communicate with the peripheral AER readout circuits are not shown; (F) Principle of operation. For the DAVIS240C, $C_1 = 130$ fF, and $C_2 = 6$ fF ($C_1/C_2 = 22$). For the DVS128, $C_1 = 467$ fF and $C_2 = 24$ fF ($C_1/C_2 = 20$). (Adapted from [1]).

This paper is organized as follows. Section II reviews DVS pixel circuit operation. Section III models the effects of temperature and parasitic photocurrent on the DVS pixel. Section IV compares measurements with theory. Section V concludes the paper.

II. DVS Pixel Circuit

The analog part of the original DVS pixel circuit (Fig. 1) consists of six stages: part **A** is a continuous-time photoreceptor circuit that transduces from a photocurrent (plus dark current) $I_p + I_{\text{dark}}$ to produce a voltage V_p that logarithmically increases with light intensity. Part **B** is a source follower buffer that isolates the photoreceptor from the next stage. Part **C** is a switched-capacitor differencing amplifier that amplifies the change in log intensity from the value memorized after the last event was sent. Part **D** are the two voltage comparators that detect increases or decreases in log intensity that exceed threshold values. Part **E** generates the reset pulse, including a refractory period, when the pixel receives row and column acknowledge signals RA and CA. Part **F** shows the principle of operation: Reset momentarily connects switch M_r, which balances circuit C and memorizes V_{sf} across C_1. In response to a change in the continuous-time logarithmic photoreceptor

signal V_p, the pixel fires ON or OFF events when V_d goes below the ON comparator threshold or above the OFF comparator threshold. The bias currents $I_{\rm OFF} < I_d < I_{\rm ON}$ determine the event thresholds. They are generated by an on-chip proportional to absolute temperature (PTAT) bias generator [13] that uses a Widlar bootstrapped mirror master current and current splitters. The biases $I_{\rm pr}$ and $I_{\rm sf}$ are also PTAT generated currents. Each event thus signals a change of log intensity exceeding a pair of TC thresholds $\Theta_{\rm ON} > 0$ and $\Theta_{\rm OFF} < 0$

$$\Delta \ln I_p > \Theta_{\rm ON} \quad \text{or} \quad \Delta \ln I_p < \Theta_{\rm OFF}. \tag{1}$$

A variable data-rate stream of address events consisting of the addresses of the pixels and the signs of the brightness changes is output from a DVS over a digital bus interface that uses row and column arbitrations to provide access from the pixels to the shared digital output bus [12]. The stream is processed for applications using event-based algorithms and hardware architectures [11], [12].

III. Theory of DVS Temperature Effects

The PTAT biasing used in DVS sensors holds the subthreshold transconductances constant with temperature. However, over the range of −40 °C to +105 °C although the absolute temperature T increases by a factor of only 1.6, exponential junction leakage temperature dependencies can have a huge effect. Temperature affects DVS operation mainly in the following two ways: first, it affects the photodiode dark current leakage $I_{\rm dark}$. Dark current has two effects: it reduces contrast of real illumination signals, increasing event threshold at low illumination, and it increases shot noise at low illumination, increasing the jitter in event timing and causing temporal noise events. Dark current doubles about every 6-8 °K [14], [15], resulting in an increase of about 50× from room temperature to +60 °C. Second, temperature also affects the junction leakage in the reset transistor M_r ($I_{\rm leak}$ in diode DL in Fig. 1). As explained later, this current generates ON events. Hence, we expect that leak event ON activity will double every 6–8 °K increase in temperature, as analyzed in Section III-B1.

A. Analysis of Temperature Dependence of Event Threshold

We will now derive the condition for generating ON and OFF events in the DVS pixel of Fig. 1. This analysis shows the interesting result that TC threshold is independent of temperature, when the I_d, $I_{\rm ON}$, and $I_{\rm OFF}$ bias currents have a fixed ratio. In this analysis, we use the subthreshold n-FET saturation current $I_{\rm ds}$ given by

$$I_{\rm ds} = I_0 \exp\left(\frac{\kappa_n V_{\rm g} - V_s}{U_T}\right) \tag{2}$$

where I_0 is the OFF current, κ_n is the n-FET back-gate coefficient, V_g and V_s are the gate and source voltages, and $U_T = kT/q$ is the thermal voltage [16]. We assume that transistors operate in subthreshold, that photocurrent is much larger than dark current, and that switches cause no charge injection.

If the pixel just generated an event, then the log intensity information was memorized across the capacitor C_1 and M_r is turned OFF. Future changes ΔV_p, $\Delta V_{\rm sf}$, and ΔV_d in response to a change $\Delta \ln I_p$ of the log photocurrent are given by

$$\begin{aligned} \Delta V_p &= \frac{U_T}{\kappa_n} \Delta \ln I_p, \quad \Delta V_{\rm sf} = \kappa_p \Delta V_p \\ \Delta V_d &= \frac{-C_1}{C_2} \Delta V_{\rm sf} = -\frac{C_1 \kappa_p U_T}{C_2 \kappa_n} \Delta \ln I_p. \end{aligned} \tag{3}$$

The differencing amplifier closed loop gain is the capacitor ratio $C_1/C_2 \approx 20$. κ_n and κ_p are the back gate coefficients of n and p FET transistors. These κ depend slightly on operating point but are assumed to be constant values.

Equation (3) shows that ΔV_d is PTAT, which is a result of the effect of temperature on the $M_{\rm fb}$ transconductance. Using a fixed voltage threshold to detect events would result in temperature dependent contrast threshold. At higher temperature, the threshold contrast would be lower.

If the differencing amplifier and comparators are biased with fixed currents $I_{\rm ON} > I_d > I_{\rm OFF}$, then at the balance point (in reset), $M_{\rm dp}$ is diode connected and conducts the current $I_{\rm dp} = I_d$. Thus the condition that an ON or OFF event is generated is the same as the condition that $I_{\rm dp}$ becomes larger than $I_{\rm ON}$, or less than $I_{\rm OFF}$. For ON events this condition becomes

$$\begin{aligned} I_{\rm dp} &> I_{\rm ON} \\ I_d \exp(-\kappa_p \Delta V_{d,\rm th}/U_T) &> I_{\rm ON} \end{aligned} \tag{4}$$

where $\Delta V_{d,\rm th}$ represents the critical change in V_d required to signal an ON event, i.e., a "threshold change" in V_d. In other words, the $I_{\rm dp}$ current must increase to become larger than the static ON comparator amplifier bias current $I_{\rm ON}$. The required decrease $\Delta V_{d,\rm th}$ of the amplifier output voltage is specified by (4).

Solving inequality (4) for $\Delta V_{d,\rm th}$ obtains it in terms of the bias currents I_d and $I_{\rm ON}$. We then use (3) to relate ΔV_d to $\Delta \ln I_p$, and obtain the threshold TC $\Theta_{\rm ON}$ in (5). The $\Theta_{\rm ON}$ is the threshold change in log intensity $\Delta_{\rm th} \ln I_p$ that causes a threshold voltage change $\Delta V_{d,\rm th}$

$$\begin{aligned} -\Delta V_{d,\rm th} &= \frac{U_T}{\kappa_p} \ln \frac{I_{\rm ON}}{I_d} = -\frac{C_1 \kappa_p U_T}{C_2 \kappa_n} \Delta_{\rm th} \ln I_p \\ \Theta_{\rm ON} \Delta_{\rm th} \ln I_p &= \frac{\kappa_n C_2}{\kappa_p^2 C_1} \ln \frac{I_{\rm ON}}{I_d} \end{aligned} \tag{5}$$

where $\Delta V_{d,\rm th}$ is a PTAT voltage, but because the photoreceptor transimpedance is also PTAT, the threshold contrast $\Theta_{\rm ON}$ is temperature independent if $I_{\rm ON}/I_d$ is constant with temperature.

Similarly, the OFF event TC threshold $\Theta_{\rm OFF}$ is given by ($\Theta_{\rm OFF}$ is negative because $I_{\rm OFF}$ is smaller than I_d)

$$\Theta_{\rm OFF} = \frac{\kappa_n C_2}{\kappa_p^2 C_1} \ln \frac{I_{\rm OFF}}{I_d}. \tag{6}$$

If $|\Theta| << 1$, then it can be expressed as a relative or percentage change of illumination using the approximation $\ln(1+\varepsilon) \approx \varepsilon$ when $\varepsilon << 1$.

Because the photoreceptor gain and comparator thresholds both scale with U_T, it cancels out. Thus, we obtain the result that Θ_{ON} and Θ_{OFF} depends on the ratios of bias currents.

Measurements of the bias current ratios are shown in Fig. 6 and are discussed in relation to the threshold measurements of Section IV-D.

DVS variants with increased front-end gain [4], [6], [8], [10] should have no effect on the temperature dependence of the thresholds, since increased gain does not change the factor of U_T in the transimpedance of the logarithmic photoreceptor, i.e., increased front-end gain is equivalent to increased C_2/C_1 ratio in (5) and (6).

B. Effects of Junction Leakage

Temperature affects junction leakage current. This leakage affects the threshold TC, and it generates a background DVS activity of ON events. These effects are analyzed in the following.

Junction leakage and dark current are exponentially dependent on temperature. Junction leakage is often fit by an Arhenius function

$$I_{leak} \propto \exp(-E_a/kT) \tag{7}$$

where I_{leak} is the leakage current, E_a is an activation energy, k is Boltzmann's constant, and T is absolute temperature [15]. Typically, E_a has a value of ranging from 1.0 eV down to 0.5 eV.

From (7) we obtain

$$\ln I_{leak} = \text{constant} - \frac{E_a}{kT}. \tag{8}$$

It shows that the slope of the log junction leakage effect plotted versus $1/kT$ yields the activation energy E_a.

Section IV-B shows measurements of these effects.

1) Leak Events Caused by Junction Leakage: An important junction leakage current labeled I_{leak} in Fig. 1 is the DL reverse diode leakage from n-well to source–drain node V_r of M_r in the differencing amplifier. It injects charge onto the V_r floating input node of the amplifier. The differencing amplifier acts as a charge-sense amplifier, where C_2 is the sense capacitance. This current causes V_d to fall, as if the light intensity were constantly rising. Following a similar analysis as for (5), a "leak event" is generated when the integrated charge on the sense capacitor C_2 causes a change exceeding the threshold, $\Delta V_{d,th}$ from (5). Calculating the time interval from reset for this event results in

$$\frac{I_{leak}\Delta t_{leak}}{C_2} = \Delta V_{d,th} \tag{9}$$

where Δt_{leak} is the time required to generate a leak event. Since the leak event firing rate is very low, the refractory period can be ignored. The leak event firing rate f_{leak} is given by

$$f_{leak} = \frac{1}{\Delta t_{leak}}. \tag{10}$$

In published DVS sensors, at room temperature the leak rate is about 0.1 Hz [1], [3], equivalent to an I_{leak} of about 10^3 e/s. At a given temperature, the leak events are uncorrelated between pixels. They are easily filtered out at low algorithmic [17] or logic cost [18]. At increased temperature, the rate becomes high enough that it can disturb tracking or feature detection even after filtering. Therefore, it is useful to consider these events.

The leak can be considered as a continuous fictional increase of log intensity. The leak thus increases the rate of ON events and decreases the rate of OFF events. Combining (3) with (9) results in the useful expression (11) for the fictitious leak TC TC_{leak}

$$TC_{leak} = \left.\frac{d \ln I_p}{dt}\right|_{leak} = \frac{\kappa_n}{\kappa_p}\frac{I_{leak}}{C_1 U_T} = \frac{f_{leak}}{\Theta_{ON}}. \tag{11}$$

Equation (11) provides a simple interpretation of the leak activity as a fictitious TC increase where each leak event signals a relative increase of intensity of the threshold amount. At room temperature, assuming $I_{leak} = 10^3$e/s and $C_1 =$ 200 fF thus results in an output that is equivalent to 0.6%/s of brightness increase. Equivalently, a 0.1 Hz leak rate with 15% TC threshold ($\Theta_{ON} = 0.15$) is also 0.66%/s fictitious increase.

2) Leak Activity Caused by Parasitic Photocurrent: The M_r transistor switch can also generate unintended parasitic photocurrent I_{par} across DL in parallel with I_{leak} that is caused by light that either penetrates the overlying metal shield or that scatters into the n-well. This light generates electron-hole pairs in the n-well and p-type M_r source–drain that cause a photocurrent in DL like the reverse junction leakage I_{leak}. This parasitic photocurrent generates DVS ON events in conditions of dc illumination. Because this effect is generally unnoticeable in indoor or laboratory lighting conditions, it has not been previously characterized. The analysis of this effect is the same as for leak events of Section III-B1. The event rate caused by I_{par} depends on the threshold.

A dimensionless measure of I_{par} is defined by estimating the parasitic photocurrent quantum efficiency QE_{par}. It is the fraction of photons hitting the pixel that generate a parasitic photocurrent electron. From (11), I_{par} is estimated using the measured parasitic photocurrent event rate f_{par} using

$$I_{par} = \frac{\kappa_p}{\kappa_n}\frac{f_{par}}{\Theta_{ON}} C_1 U_T. \tag{12}$$

Then QE_{par} is estimated using the measured incident flux striking the pixel and I_{par}

$$QE_{par} = \frac{I_{par}/q}{\#\ \text{photons/sec}}. \tag{13}$$

Section IV-C presents measurements of (13) from several sensors.

IV. Measurements of Temperature Effects

To control device temperature, we used a thermal wand (Temptronic ThermoStream TP41000A). Device temperature was measured either with thermocouple or with the integrated inertial measurement unit.

We mainly tested two different DVS-type sensors in these experiments, the DVS128 [1] and the DAVIS240C (second generation of [3]). The DVS128 and DAVIS240C are commercially available as research and development prototypes

from inilabs. We tested parasitic photocurrent effects in two additional unpublished sensors (Section IV-C). We used the software framework jAER to control and measure these sensors [19]. We also visually compared (using the rendered camera output) the DAVIS240C with the DVS of [8]. Self-heating and thermal resistance leakage limited us to a device temperature range between 0 °C and 83 °C.

We adapted a method for TC threshold measurement established in [10] and [20]. An integrating sphere exposes the sensor to triangular LED light oscillations. Knowing the overall contrast C of the light intensity and counting the N_{ON} and N_{OFF} of ON and OFF events per pixel per edge produced in the rising and falling phases of the light, allows estimating the TC thresholds for ON and OFF events. Then the log TC thresholds are computed from

$$\Theta_{\mathrm{ON}} = \frac{\ln C}{N_{\mathrm{ON}} + 1}, \quad \Theta_{\mathrm{OFF}} = -\frac{\ln C}{N_{\mathrm{OFF}} + 1}. \tag{14}$$

The 1 is added to each event count because pixels on average fire one less event because of quantization. At the start of a cycle and end of a phase, the pixel is on average halfway to and from the threshold. This correction has been validated by behavioral pixel simulations available on request.

The noise recorded during dc lighting is used to estimate the leak and random temporal noise event activity.

A. DAVIS240 Example Data Over Temperature Range

The DAVIS240C is a 240 × 180 pixel DAVIS APS-DVS camera [3]. The pixel circuit of the DAVIS allows simultaneously detecting and outputting DVS events while synchronously outputting conventional active pixel sensor (APS) image frames.

Fig. 2 shows snapshots of APS images and overlaid 2-D event histograms of a moving Edmund density step chart collected from the DAVIS240C camera at various T using the same bias current settings for all T. This chart has 10 steps of 0.1 density. Each step has a contrast of $10^{0.1} = 1.26$. The sensor output is nearly unchanged over this temperature range, in agreement with theory. The following sections quantitatively measures effects over temperature.

B. Measurements of Dark Current and Leak Event Activity

Fig. 3 shows steady-state photodiode dark current and leak event rate as a function of temperature plotted as the log of the quantity versus reciprocal of absolute temperature. The temperature axis is labeled with centigrade. The photodiode dark current was measured in the dark. For DVS128 we had access to sum of photocurrents; for DAVIS240 we used APS dark current droop rate of APS signal and measured conversion gain. Leak event activity was measured by counting the events generated under a uniform low (<100 lux) dc light illumination. Two sensors, the DVS128 [Fig. 3(A)] and DAVIS240C [Fig. 3(B)] were measured. DVS128 was built in 350-nm mixed signal RF technology and DAVIS240C was built in 180-nm CMOS image sensor technology.

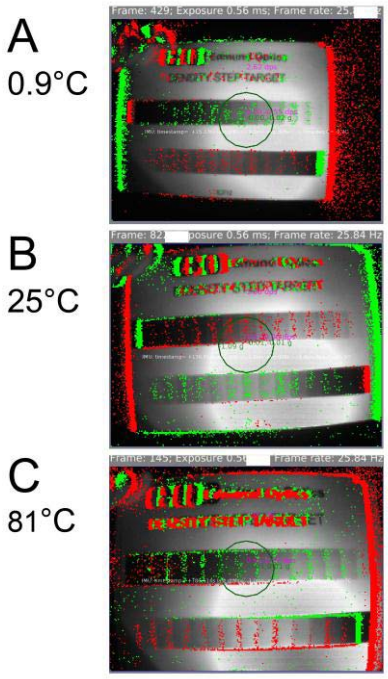

Fig. 2. (A)–(C) DAVIS240C 40 ms snapshots of frames and events collected at various temperatures viewing moving Edmund density step chart. ON events are green, and OFF events are red. Bias settings were left untouched (I_d = 39.5 nA, I_{ON} = 1.8 uA, and I_{OFF} = 1.9 nA). Full scale is one event. APS exposure duration: 1.1 ms. Scene illumination: Incandescent, 550 lux, 8.1 W/m^2. Lens: 4.5 mm f/1.4.

The sensors have comparable photodiode dark current activation energies ($E_{a,\mathrm{dark}}$ 0.54 eV versus 0.60 eV) and leak activity $E_{\mathrm{a,leak}}$ (0.73 eV versus 0.88 eV). The model of (7) is valid over a range extending from about 15 °C to 60 °C. The DVS128 dark current at room temperature is 4 fA, or about 10 nA/cm^2 of photodiode area. The DAVIS240C dark current is reduced by a factor of more than 10 × to 0.34 fA (0.45 nA/cm^2) because of the improved photodiodes.

Below 20 °C the leak activity stops decreasing with temperature due to leak events generated by parasitic photocurrent in the M_r junction from the dc illumination used in the experiment.

The DVS128 uses an n-well photodiode with a large depletion width. The low activation energy of the dark current is consistent with depletion region dominated generation [21, PP. 172–180]. Likewise, the higher activation energy of the leak activity is consistent with a mixture of depletion and diffusion generation in the one-sided p-FET source/drain junction. The DAVIS240C uses a surface photodiode with improved quantum efficiency and smaller dark current than the n-well photodiode of the DVS128, but the activation energy is similar, indicating similar generation processes.

C. Measurement of Events Generated by Parasitic Photocurrent

We measured the dc event rate generated by parasitic photocurrent (Section III-B2), and then estimated the effective $\mathrm{QE}_{\mathrm{par}}$ for the DL parasitic photodiode (Fig. 1). Fig. 4 shows

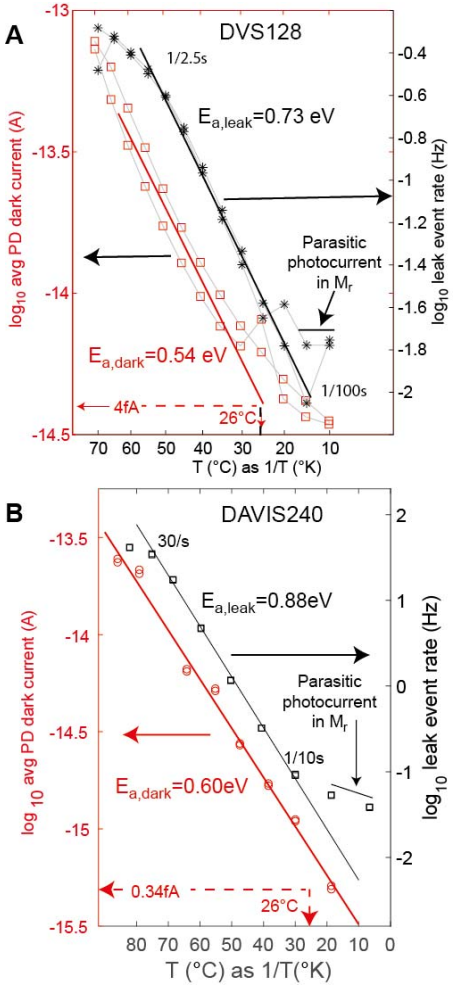

Fig. 3. (A) and (B) Log leak activity per pixel rate and the log photodiode dark current as a function of 1/T(K) for (A) DVS128 and (B) DAVIS240C cameras. The thin gray lines in (A) show the order of measurements in the up and down sweep of temperature. *Y*-axis scales differ for dark and leak activities.

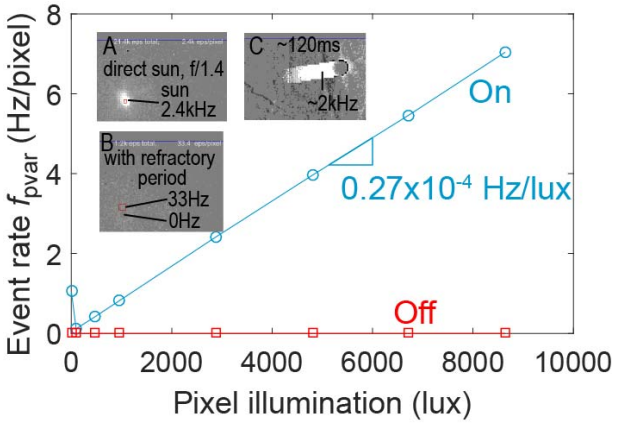

Fig. 4. Parasitic photocurrent-induced events versus incident illumination for DAVIS240C. Temporal noise at low light intensity increases the count. The OFF rate is zero for nearly all points. Insets show the rate for direct solar imaging using $f/1.4$ lens with (A) short and (B) long refractory period setting. (C) Trail of ON events left behind the moving sun.

TABLE I
PARASITIC PHOTOCURRENT MEASUREMENTS

Sensor	f_{par}/lux (Hz/pixel/lux) With Θ_{on}=0.3	QE_{par}
DVS128	2.87×10^{-4}	9.5×10^{-6}
DAVIS240C	2.70×10^{-4}	1.1×10^{-5}
DAVIS346	6.65×10^{-4}	2.8×10^{-5}
BSIDAVIS346	1.44×10^{-3}	6.0×10^{-5}

the DAVIS240C dc event rate versus incident illumination using the same biases as for the TC threshold measurements in the next section. From the intercept of this measurement, we estimated the leak event rate f_{leak} and subtracted it from the measured frequencies to obtain the parasitic photocurrent event rate f_{par}. From f_{par} and the known C_1 (see Fig. 1) and measured event threshold value Θ_{ON}, we used (12) to compute I_{par}. We used the measured irradiance and (13) to compute QE_{par}.

We measured the DVS128, the DAVIS240C, and two additional unpublished sensors, the DAVIS346 and the BSIDAVIS346; their pixel circuits are almost identical with the DAVIS240C, but their M_r DL is not salicided. The BSIDAVIS346 has the same CMOS circuits as DAVIS346 but is fabricated on 18-μ m-thick p-epi and was postprocessed for back-illumination. Since the BSIDAVIS346 is back-illuminated, it is more sensitive to I_{par} effects. Table I summarizes the parasitic photocurrent measurements.

The QE_{par} for the front illuminated sensors means that only a few out of 10^5 photons hitting the pixel generates an electron in the M_r source–drain DL diode. The area of DL is about $(0.5um)^2/(18.5um)^2 \approx 10^{-3}$ of the total pixel area in the DAVIS pixels. Thus only about 1% of the photons striking in the DL area cause a collected photoelectron. The QE_{par} of the DAVIS346 is about 3 times that of the DAVIS240C. Since the layouts are nearly identical, we speculate that the higher QE_{par} in the DAVIS346 is from its unsalicided DL compared with the normal salicided DL on the DAVIS240. The back-illuminated sensor with $QE_{par} = 6 \times 10^{-5}$ has about twice the QE_{par} of the front illuminated version (about 3×10^{-5}); it is surprising that it is only twice as high but this could be due to the absence of near infrared illumination in the LED stimulus. Visible light with wavelength of 730 nm (the limit of the LED output) has an attenuation length of about 3 μm [22], which is much less than the 18-μ m-epi thickness.

A useful metric is the parasitic photocurrent event rate [f_{par}, (12)] versus incident illumination, at a specified threshold. Only bright light sources or specular reflections of sunlight cause visually noticeable parasitic dc events. In our experience, accidental solar imaging often occurs in driving, outdoor surveillance and drone applications. Imaging the 10^9 cd/m^2 solar disk at noon using a lens with aperture ratio of $f/8$ (typical for bright lighting situations) produces an illuminance of the sensor of about 10^7 lux. We used a faster f/1.4 lens to image the sun and observed a significant f_{par} of about 2.4 kHz [Inset Fig. 4(A)] when we increased the I_{refr} bias current sufficiently (circuit E of Fig. 1). Using a longer refractory period, we could limit the rate (for all pixels

including the sun-illuminated ones) to about 30 Hz [Inset Fig. 4(B)]. Here, DVS events are completely suppressed at the center of the sun. We speculate that this suppression is due to parasitic photocurrent toward ground in the n-FET transistors M_{a1} and M_{a2}. If this current is larger than I_{refr}, then it holds affected pixels permanently in reset. The trail of ON events behind the moving sun in Fig. 4(C) is not explained.

Light sources other than the sun generate much lower event rates. A white beach or snow field at noon and car headlamps is less than 10^5 cd/m^2, producing about 10^4 lux at the sensor with a fast lens. The parasitic photocurrent events from bright sky or ground parts of sunlit scene of the Fig. 4 insets are about 1 Hz, and like the leak events, are uncorrelated and easily filtered out.

D. Measurement of Temporal Contrast Threshold Over Temperature

The setup used to compute TC threshold is the same as the one used in measurements for background event and dark current for the DAVIS240C. ON and OFF events were recorded from the sensor while a 0.4 Hz triangular wave with 50 lx/250 lx min/max illumination (contrast $C = 5$) was shined onto the sensor. The thresholds were then computed from (14). The 0.4 Hz frequency compromises between low frequency (where leak events cause a larger effect) and high-frequency (where the address-event representation (AER) output bus tends to saturate with this global stimulation).

We used bias current values that provided functional sensor operation over the entire temperature range (see Fig. 2). Event activity was dominated by response to the illumination change, so that during the rising illumination phase, the sensor output was dominated by ON activity and during the falling phase by OFF activity.

Fig. 5 shows the results of these measurements. Fig. 5(A) shows the event count per pixel per edge (rising or falling) of the triangular LED stimulus. The On and Off counts are plotted for both rising and falling phases. Fig. 5(B) plots the On rising and Off falling data using (14). As mentioned earlier, TC threshold is ideally temperature independent, which is observed over much of the temperature range. However, the TC threshold has some temperature dependence due to junction leakage current in the reset transistor [Fig. 1(C)], which contributes to ON events. Since this leakage current has temperature dependence as described in Section III-A, we can expect to observe more ON events and fewer OFF events with a rise in temperature, particularly at the low temporal frequency used for this measurement.

The TC used here varies over a factor of five from $dI/dt/I = (200\text{lx}/1.25\text{s})/50\text{lx}=3.2/\text{s}=320\%/\text{s}$ at the minimum intensity to 64%/s at the maximum intensity. The fictitious leak TC at room temperature is about 1%/s from (11). It increases about 50× at the highest temperature to become comparable with the smallest TC of the stimulus. That explains why the threshold measurement of Fig. 5 is not affected by elevated leak event activity except at the highest temperature. The small increase in thresholds at low temperature is not understood.

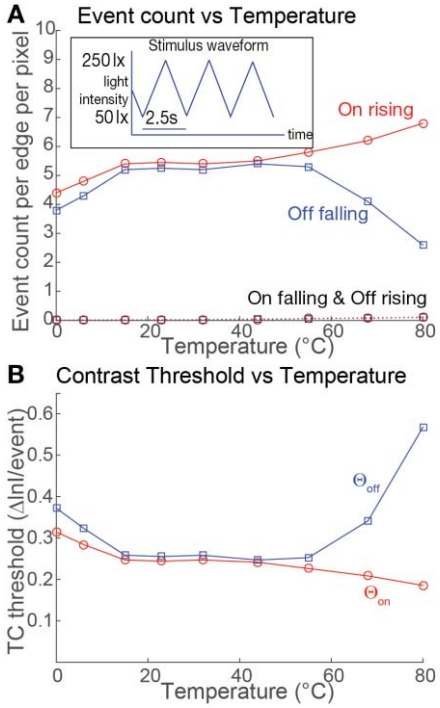

Fig. 5. DAVIS240C TC threshold versus temperature. (A) Event count per pixel per edge for 5× contrast triangular input. Plots the event count for rising and falling phases for both types of events. (B) TC threshold computed from (14). Biases used were the same as for Fig. 2 data.

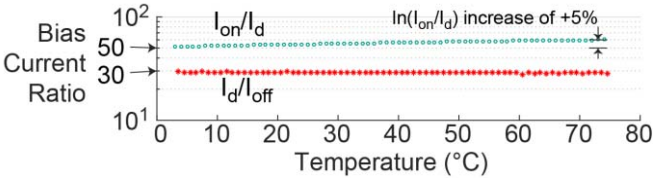

Fig. 6. Measured bias current ratios.

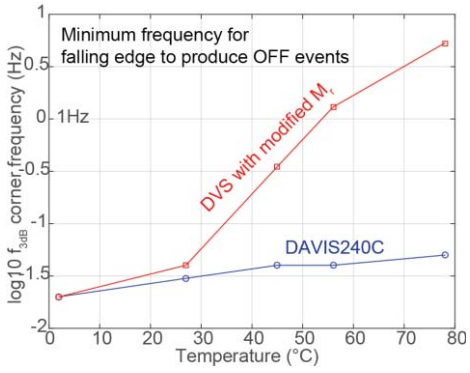

Fig. 7. Measured high-pass corner frequency versus temperature for original DVS versus DVS of [8].

Fig. 6 shows measurements of the validity of ratio biasing in the DVS pixel in (5) and (6). It plots the measured bias current ratios from the bias generator [13] versus temperature. A log plot is used because the TC threshold is proportional to the log ratio from (5) and (6). The ratios are nearly constant, showing constant ratio biasing is a valid assumption. These measured bias current ratios in (5) and (6), assuming

$\kappa_n = \kappa_p = 0.7$ and $C_2/C_1 = 22$ (Fig. 1), result in $\Theta_{ON} = +0.27$ and $\Theta_{OFF} = -0.22$. These thresholds are close to the measured values in Fig. 5(B) of about ± 0.25. All currents are derived by current splitters from a master current. The reason that $\ln(I_{ON}/I_d)$ increases by 5% but I_{OFF}/I_d is almost constant over this range is unknown. However, this small change has no impact on DVS thresholds that we could measure.

V. Discussion and Conclusion

To reduce leak events, [8] proposed connecting the M_r bulk to V_d. After reset, the M_r bulk–source voltage is zero, so junction leakage is eliminated, but not parasitic photocurrent. This connection increases the $V_{ds} = 0$ M_r conductance by a factor $\exp[((1-\kappa_p)(V_{dd} - V_d)/U_T)] \approx 31$ when $V_{dd} - V_d = 0.3$ V and $\kappa = 0.7$. It thus increases the high-pass corner frequency, especially at elevated temperature. Fig. 7 compares the measured corner frequency of DAVIS240C and the sensor in [8] versus temperature. However, this effect may be worth the cancellation of leak events at all temperatures.

This paper discussed the theory and measurement of DVS temperature effects. It shows that the DVS TC threshold is independent of temperature if there is no junction leakage current and ratios of bias currents are constant with temperature. At elevated temperatures, junction leakage plays a significant role in raising the apparent threshold for OFF events while lowering it for ON events. Across two different silicon processes, both dark current and transistor junction leakage current closely follow an exponential activation energy model. A new metric QE_{par} was defined and measured for parasitic photocurrent-induced DVS events.

Acknowledgment

The authors would like to thank S. Bamford, F. Corradi, C. Li, L. Longinotti, and D. Moeys for technical assistance and Samsung for the use of their prototype.

References

[1] P. Lichtsteiner, C. Posch, and T. Delbruck, "A 128×128 120 dB 15 μs latency asynchronous temporal contrast vision sensor," *IEEE J. Solid-State Circuits*, vol. 43, no. 2, pp. 566–576, Feb. 2008.

[2] C. Posch, D. Matolin, and R. Wohlgenannt, "A QVGA 143 dB dynamic range frame-free PWM image sensor with lossless pixel-level video compression and time-domain CDS," *IEEE J. Solid-State Circuits*, vol. 46, no. 1, pp. 259–275, Jan. 2011.

[3] C. Brandli, R. Berner, M. Yang, S.-C. Liu, and T. Delbruck, "A 240×180 130 dB 3 μs latency global shutter spatiotemporal vision sensor," *IEEE J. Solid-State Circuits*, vol. 49, no. 10, pp. 2333–2341, Oct. 2014.

[4] J. A. Lenero-Bardallo, T. Serrano-Gotarredona, and B. Linares-Barranco, "A 3.6 μs latency asynchronous frame-free event-driven dynamic-vision-sensor," *IEEE J. Solid-State Circuits*, vol. 46, no. 6, pp. 1443–1455, Jun. 2011.

[5] C. Li *et al.*, "Design of an RGBW color VGA rolling and global shutter dynamic and active-pixel vision sensor," in *Proc. IEEE Int. Symp. Circuits Syst. (ISCAS)*, Vaals, The Netherlands, May 2015, pp. 718–721.

[6] T. Serrano-Gotarredona and B. Linares-Barranco, "A 128×128 1.5% contrast sensitivity 0.9% FPN 3 μs latency 4 mW asynchronous frame-free dynamic vision sensor using transimpedance preamplifiers," *IEEE J. Solid-State Circuits*, vol. 48, no. 3, pp. 827–838, Mar. 2013.

[7] M. Yang, S.-C. Liu, and T. Delbruck, "A dynamic vision sensor with 1% temporal contrast sensitivity and in-pixel asynchronous delta modulator for event encoding," *IEEE J. Solid-State Circuits*, vol. 50, no. 9, pp. 2149–2160, Sep. 2015.

[8] B. Son *et al.*, "A 640 × 480 dynamic vision sensor with a 9 μm pixel and 300 Meps address-event representation," in *IEEE Int. Solid-State Circuits Conf. (ISSCC) Dig. Tech. Papers*, San Francisco, CA, USA, Feb. 2017, pp. 66–67.

[9] T. Delbruck, "Neuromorphic vision sensing and processing," in *Proc. 46th Eur. Solid-State Device Res. Conf.*, Lausanne, Switzerland, Sep. 2016, pp. 7–14.

[10] D. P. Moeys, "Analog and digital implementations of retinal processing for robot navigation systems," Ph.D. dissertation, Dept. Elect. Inf. Eng. (D-ITET), ETH Zurich, Zurich, Switzerland, 2017.

[11] C. Posch, T. Serrano-Gotarredona, B. Linares-Barranco, and T. Delbruck, "Retinomorphic event-based vision sensors: Bioinspired cameras with spiking output," *Proc. IEEE*, vol. 102, no. 10, pp. 1470–1484, Oct. 2014.

[12] S.-C. Liu, T. Delbruck, G. Indiveri, A. M. Whatley, and R. Douglas, Eds., *Event-Based Neuromorphic Systems*. New York, NY, USA: Wiley, 2015.

[13] M. Yang, S.-C. Liu, C. Li, and T. Delbruck, "Addressable current reference array with 170 dB dynamic range," in *Proc. IEEE Int. Symp. Circuits Syst. (ISCAS)*, May 2012, pp. 3110–3113.

[14] R. Widenhorn, M. M. Blouke, A. Weber, A. Rest, and E. Bodegom, "Temperature dependence of dark current in a CCD," *Proc. SPIE*, vol. 4669, pp. 193–201, Apr. 2002.

[15] P. R. Gray, P. J. Hurst, S. H. Lewis, and R. G. Meyer, *Analysis and Design of Analog Integrated Circuits*, 4th ed. Hoboken, NJ, USA: Wiley, 2001.

[16] C. A. Mead, *Analog VLSI and Neural Systems*, 1st ed. Reading, MA, USA: Addison-Wesley, 1989.

[17] T. Delbruck, "Frame-free dynamic digital vision," in *Proc. Int. Symp. Secure-Life Electron.*, Tokyo, Japan, vol. 1. 2008, pp. 21–26.

[18] A. Linares-Barranco, F. Gómez-Rodríguez, V. Villanueva, L. Longinotti, and T. Delbrück, "A USB3.0 FPGA event-based filtering and tracking framework for dynamic vision sensors," in *Proc. IEEE Int. Symp. Circuits Syst. (ISCAS)*, May 2015, pp. 2417–2420.

[19] (Mar. 23, 2007). *JAER Open Source Project*, accessed on May 23, 2016. [Online]. Available: http://jaerproject.org

[20] R. Berner, "Building blocks for event-based sensors," Ph.D. dissertation, Dept. Inf. Technol. Elect. Eng. (D-ITET), Univ. Zurich, Zürich, Switzerland, 2011.

[21] A. S. Grove, *Physics and Technology of Semiconductor Devices*. New York, NY, USA: Wiley, 1967.

[22] W. C. Dash and R. Newman, "Intrinsic optical absorption in single-crystal germanium and silicon at 77°K and 300°K," *Phys. Rev.*, vol. 99, no. 4, pp. 1151–1155, Aug. 1955.

Yuji Nozaki is currently pursuing the Ph.D. degree with the Department of Computational Intelligence and Systems Science, Tokyo Institute of Technology, Tokyo, Japan.

His current research interests include event-based vision sensors and internal representations in multilayer networks.

Tobi Delbruck (M'99–SM'06–F'13) is currently a Professor with the Institute of Neuroinformatics, University of Zurich, and ETH Zürich, Zürich, Switzerland. His current research interests include neuromorphic event-based sensors, sensory processing, and deep neural network inference theory and hardware.

Dr. Delbruck is a past Chair of the IEEE CAS Sensory Systems Technical Committee.